

Article

Accuracy–Power Controllable LiDAR Sensor System with 3D Object Recognition for Autonomous Vehicle

Sanghoon Lee ^{1,2}, Dongkyu Lee ², Pyung Choi ² and Daejin Park ^{2,*}¹ Carnavicom Co., Ltd., Incheon 21984, Korea; shlee@carnavi.com² School of Electronic and Electrical Engineering, Kyungpook National University, Daegu 41566, Korea; dklee1215@knu.ac.kr (D.L.); p0choi@ee.knu.ac.kr (P.C.)

* Correspondence: boltanut@knu.ac.kr; Tel.: +82-53-950-5548

Received: 7 August 2020; Accepted: 4 October 2020; Published: 7 October 2020



Abstract: Light detection and ranging (LiDAR) sensors help autonomous vehicles detect the surrounding environment and the exact distance to an object's position. Conventional LiDAR sensors require a certain amount of power consumption because they detect objects by transmitting lasers at a regular interval according to a horizontal angular resolution (HAR). However, because the LiDAR sensors, which continuously consume power inefficiently, have a fatal effect on autonomous and electric vehicles using battery power, power consumption efficiency needs to be improved. In this paper, we propose algorithms to improve the inefficient power consumption of conventional LiDAR sensors, and efficiently reduce power consumption in two ways: (a) controlling the HAR to vary the laser transmission period (T_p) of a laser diode (LD) depending on the vehicle's speed and (b) reducing the static power consumption using a sleep mode, depending on the surrounding environment. The proposed LiDAR sensor with the HAR control algorithm reduces the power consumption of the LD by 6.92% to 32.43% depending on the vehicle's speed, compared to the maximum number of laser transmissions ($N_{x,max}$). The sleep mode with a surrounding environment-sensing algorithm reduces the power consumption by 61.09%. The algorithm of the proposed LiDAR sensor was tested on a commercial processor chip, and the integrated processor was designed as an IC using the Global Foundries 55 nm CMOS process.

Keywords: LiDAR sensor processor; low-power circuit design; 3D object recognition; autonomous vehicle

1. Introduction

With the rapid development of automotive technology, the types and quantities of sensors mounted on automobiles are gradually increasing, and the quantitative and qualitative improvement of sensors provides safety and convenience for drivers and passengers [1–3]. Therefore, because recently developed autonomous vehicles use a large number of various sensors, research has focused on the safety of and convenience for drivers, as well as on fusion signal processing among a number of used sensors [4,5]. Among the sensors that provide safety and convenience, light detection and ranging (LiDAR) sensors are the most essential for autonomous vehicles because they measure the distance between a vehicle and an object and recognize the object [6,7]. As shown in Figure 1, a typical LiDAR sensor using a laser in 905 nm of the near-infrared ray (NIR) region uses technology to convert the time-of-flight (ToF), which is the time difference between the transmission of the laser (t_1) and its reflection from an object back to the sensor (t_2) [8–11].

A LiDAR sensor, which detects the exact distance from an object by transmitting a laser, consists of a laser diode (LD), an avalanche photo diode (APD), a time-to-digital converter (TDC), and signal processing units, as shown in Figure 2 [12].

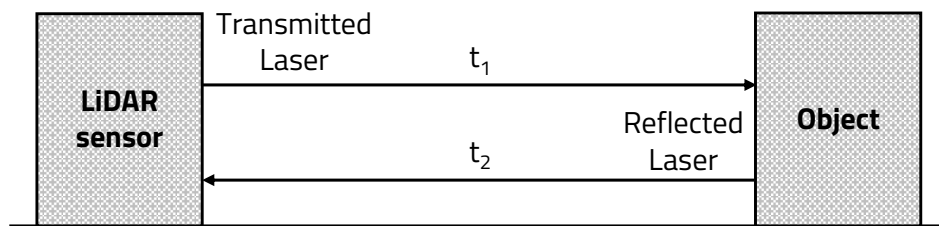


Figure 1. Time-of-flight (ToF) of laser.

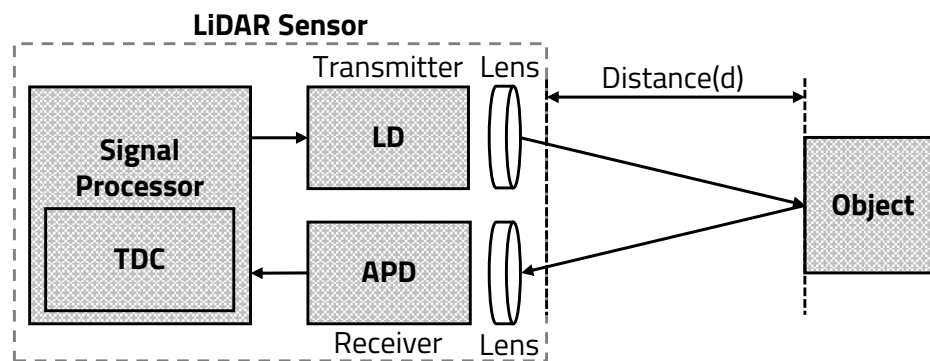


Figure 2. Structure and operation of conventional light detection and ranging (LiDAR) sensor.

The LD transmits the laser, which is focused through a light transmitting lens. The laser transmitted from the LD is reflected back from the object and received by the APD through the light-receiving lens. The TDC measures the difference between the time the LD transmits the laser and the time the APD receives it, and then converts the difference to the ToF. The signal-processing unit, denoted by a microprocessor (MP), receives the ToF from the TDC and calculates the distance between the LiDAR sensor and the object.

The laser of the LiDAR sensor can be classified into a pulsed, amplitude-modulated continuous-wave (AMCW), and frequency-modulated continuous-wave (FMCW) according to the transmission principle. The pulsed is a method of transmitting a laser with an instantaneous peak power using a short pulse of several nanoseconds. Because an intensity of an instantaneous laser is strong, it is used for long distance measurement. The AMCW is a method of transmitting a continuous laser. The distance is measured by comparing phases of the transmitted and backscattered detected waves. Because it measures a phase shift of the transmitted and received laser, it is not suitable for an accurate distance and long distance measurement [13]. The FMCW is a method that compensates for AMCW's incorrect distance measurement. It transmits the laser continuously, but the frequency changes with time. The accurate distance measurement is possible because the laser transmission time can be known through the frequency of the received signal. However, it is structurally more complex than the AMCW and is not suitable for the long distance measurement because the frequency changes due to the Doppler effect [14].

The types of LiDAR sensors that measure distance are categorized into scanning sensors, microelectromechanical system (MEMS) sensors, flash sensors, and optical phased array (OPA) sensors. Scanning and MEMS sensors use mirrors to spread the laser to detect multiple directions. Scanning sensors use a mirror rotated by a motor to change the angle at which the laser is reflected and transmitted [15,16]. MEMS sensors use the mirror to transmit the laser in the same way as scanning sensors, but the mirror is operated vertically, horizontally, or in all directions [17–19]. Flash sensors transmit one large-area laser, such as with a digital camera, and receive the laser reflected by the object in an array sensor, which is expressed in one frame [20,21]. OPA sensors use a method in which an optical phase modulator controls a phase of the laser through the lens and transmits the laser in various directions [22,23].

In this paper, among the various types of LiDAR sensors, we use a scanning LiDAR sensor with a pulsed laser, which is best suited for autonomous vehicles requiring a wide field of view.

This paper is organized as follows. Section 2 briefly discusses the related works. Then, the problems of conventional LiDAR sensors and the method by which the proposed LiDAR sensors reduce power consumption are described in Section 3. In Section 4, the LiDAR sensor with reduced power consumption is verified through experiments. Finally, Section 5 contains the conclusion.

2. Related Works

As numerous high-tech devices are developed in various fields, miniaturization is pursued for convenience and portability. In addition, low-power issues are being discussed to enable the operation of small batteries for portability. To satisfy these requirements, the structure of the signal processing hardware has been modified in the past to reduce power consumption [24,25]. Recently, the trend is to reduce power consumption with a low-power operation algorithm and efficient data processing [26–28].

Radio detection and ranging (RADAR) sensors, similar to LiDAR sensors, have been applied in various fields for a long time, but have recently been introduced in vehicles [4]. As RADAR sensors develop in sophistication, the research on low-power consumption of RADAR sensors continues [29,30]. However, because the research period of multi-channel LiDAR sensors has not been relatively long, judging by the technology trend, the research and development of an improved sensing distance, a point-cloud signal-processing method, and accuracy and recognition are being conducted [31–34]. Because the research of a multi-channel LiDAR sensor is focused on improving performance, the research on low-power consumption for vehicles has been insufficient.

Currently, the conventional LiDAR sensors on the market have the disadvantage of inefficient power consumption because of the constant operation of a vertical angular resolution (VAR) and horizontal angular resolution (HAR) fixed. In particular, because the fatal disadvantage of the LiDAR sensor causes vulnerabilities in autonomous vehicles equipped with multiple sensors and electric vehicles using batteries as a power source, it is necessary to improve the operation method to achieve efficient power consumption [1,2]. A solution to the power consumption should be prepared according to the advanced performance of the LiDAR sensor. A simple method of reducing the power consumption involves modifying the hardware of the LiDAR sensor by focusing on an algorithm that changes the fixed accuracy of the conventional LiDAR sensor according to the condition.

The LiDAR sensor controls and changes the laser transmission period (T_p), which is the HAR, according to the vehicle's speed and surrounding environment. Because the number of laser transmissions (N_x) varies proportionally according to T_p , we propose an algorithm that can efficiently consume power according to the variable T_p [35].

3. Characteristics of Multi-Channel Scanning LiDAR Sensors

3.1. Conventional Multi-Channel Scanning LiDAR Sensors

As mentioned in the introduction, a multi-channel scanning LiDAR sensor is configured with a brushless direct current (BLDC) motor, which rotates the mirror, and an encoder within the structure of the typical LiDAR sensor, as shown in Figure 3. In addition, the multi-channel scanning LiDAR sensor uses a multi-channel APD, which determines a vertical field of view (VFoV). The encoder extracts the angle information of the BLDC motor, which rotates the mirror, and transmits it to the microprocessor (MP).

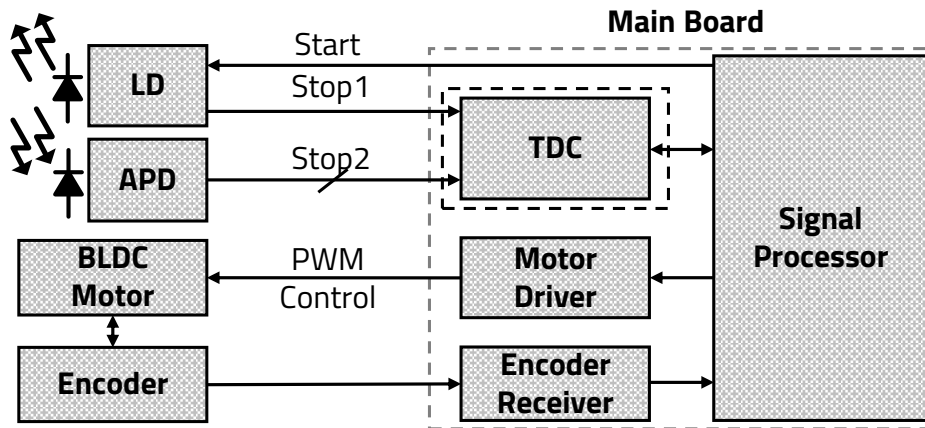


Figure 3. Block diagram of multi-channel scanning LiDAR sensor.

The MP calculates the motor’s rotation angle using the angle data received from the encoder and controls the duty cycle of a pulse width modulation (PWM) signal with the motor driver. When the mirror’s angle is in the detection range, the MP triggers a START signal to the LD. The LD, which receives the START signal from the MP, transmits a STOP1 signal to the TDC at the same time as the laser transmission. The TDC that received the STOP1 signal from the LD counts using an internal timer (TMR) until STOP2 signals from each channel of the APD come in. Each channel of the APD receives the laser reflected by the object and sends the STOP2 signal to stop the TDC from counting. The TDC transmits its count values from the STOP1 signal to the multi-channel STOP2 signal and then to the MP. After receiving the count value from the TDC, the MP converts the distance value by applying the speed of light: $C = 3 * 10^8$ m/s. The LiDAR sensor repeats these operations by the value of a horizontal field of view (HFOV) at different mirror angles.

3.1.1. Time-Domain of TDC Operations

Figure 4 shows the TDC operations process of each input signal to the TDC during the operation time and the data transmitted to the MP after signal processing [36–38].

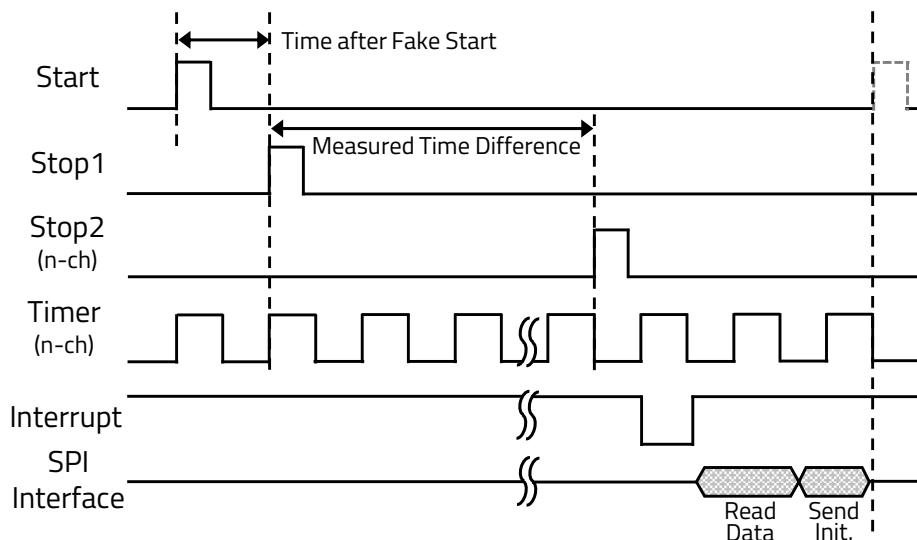


Figure 4. Time domain of time-to-digital converter (TDC).

When the MP sends the START signal to the LD and TDC, the TDC that receives the START signal waits for the STOP1 signal from the LD. The LD that received the START signal from the MP transmits the laser and sends a STOP1 signal to the TDC at the same time. When the laser reflected from the object reaches each channel of the APD, the STOP2 signals are transmitted to the TDC. The TDC’s TMR

counts from the input time of the STOP1 signal until the STOP2 signal is received by each channel of the APD. When the TMR finishes counting because all channels received STOP2 signals, the TDC sends an interrupt signal, which is the signal that reception is complete for all channels, and the ToF data of each channel are transmitted to the MP using a serial peripheral interface (SPI) communication.

3.1.2. Power Consumption of LiDAR Sensor

Figure 5 shows the overall block diagram of the LiDAR sensor when the LD of the LiDAR sensor transmits the pulsed laser once. When the LD transmits a single pulsed laser, the multi-channel APD receives the laser reflected from the object, and the received signal of the APD is transmitted and processed by the TDC and MP.

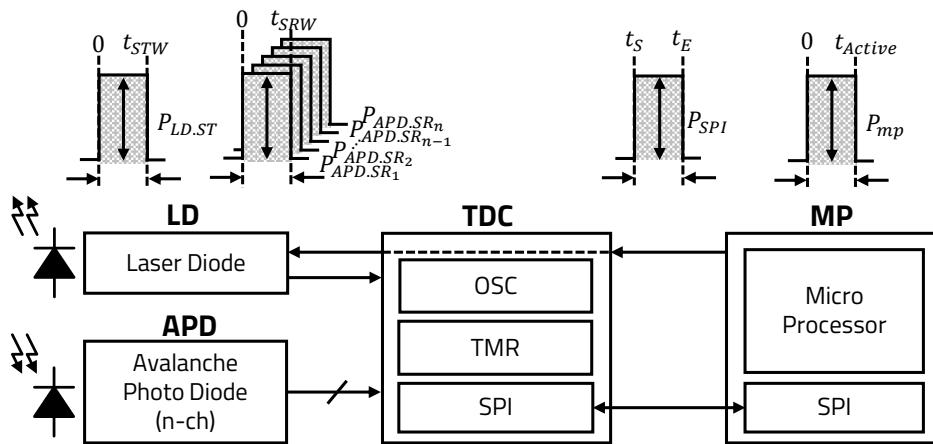


Figure 5. Power consumption of LiDAR sensor.

The energy consumption of one pulsed laser pulse transmitted from LD, as denoted by E_{LD} , is expressed as shown in Equation (1). The LD consumes dynamic power for several nanoseconds, as denoted by $P_{LD.ST}$, from the time 0, when the laser transmission starts, to the time t_{STW} , when the transmission ends. E_{LD} , which is the energy of one pulsed laser, is expressed as the integration of $P_{LD.ST}$ from 0 to t_{STW} .

$$E_{LD} = \int_0^{t_{STW}} P_{LD.ST}(t) dt \quad (1)$$

Each channel of the APD statically consumes power, as denoted by $P_{APD.SR_i}$, to recognize the laser reflected by the object. For one channel of the APD, the power consumption is the integration of $P_{APD.SR_i}$ from 0, when the reception is started, to t_{SRW} at which the reception of each channel is ended. Generally, the number of the APD's channels is determined by n cells. The total energy consumption of the APD's n channels, as denoted by E_{APD} , is expressed as the sum of the power consumption used in each channel of the APD, as shown in Equation (2).

$$E_{APD} = \sum_{i=1}^n \left[\int_0^{t_{SRW}} P_{APD.SR_i}(t) dt \right] \quad (2)$$

The TDC has an oscillator (OSC) that consumes power, as denoted by P_{OSC} , during each high-output period to count up each TMR. The energy consumption of the OSC is an integration of P_{OSC} from 0 to t_{END} when a group of data is processed. Each TMR consumes its static power, as denoted by P_{TMR_i} , when it operates from the time it receives the LD signal, as denoted by Δ_{LD} , to the time when each channel receives the APD signal, denoted by Δ_{APD_i} , as shown in Figure 6. E_{TDC}

denotes the sum of the oscillator's energy consumption and the integration of P_{TMR_i} 's power from Δ_{LD} to Δ_{APD_i} of each TMR, as shown in Equation (3).

$$E_{TDC} = \int_0^{t_{END}} P_{OSC}(t)dt + \sum_{i=1}^n \left[\int_{\Delta_{LD}}^{\Delta_{APD_i}} P_{TMR_i}(t)dt \right] \quad (3)$$

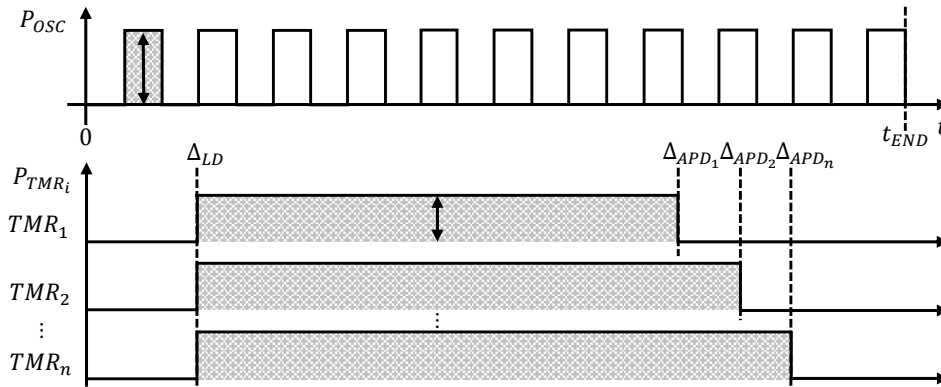


Figure 6. Power consumption of TDC.

The operating power of SPI communication, which is implemented for faster communication at the hardware level and widely used for data transmission between sensors, is also consumed during such data communication. As shown in Equation (4), the energy consumed by the SPI communication between the TDC and the MP, as denoted by E_{TP} , is expressed as the integration of the SPI's power consumption, as denoted by P_{SPI} , from the time t_S when the transmission starts to the time t_E when the transmission ends.

$$E_{TP} = \int_{t_S}^{t_E} P_{SPI}(t)dt \quad (4)$$

When the MP receives data from the TDC via the SPI communication, the MP's power consumption, as denoted by P_{MP} , is represented by Equation (5). E_P denotes the integration of the MP's instantaneous power consumption, as denoted by P_{MP} , from 0, when the data are transmitted from the TDC, to t_{Active} , when the MP completes signal processing.

$$E_P = \int_0^{t_{Active}} P_{MP}(t)dt \quad (5)$$

The LiDAR sensor's total energy consumption, as denoted by E_{Total} , is expressed as shown in Equation (6).

$$E_{Total} = E_{LD} + E_{APD} + E_{TDC} + E_{TP} + E_P \quad (6)$$

If the LiDAR sensor, which periodically transmits the laser with the certain HAR, detects objects, it consumes a constant energy as much as E_{Total} . On the other hand, if a laser transmission period of the conventional LiDAR is changed, E_{Total} will also be changed. Because the accuracy changes when T_P of the LD is varied, the LiDAR sensor is correlated with E_{APD} , E_{TDC} , and E_P . Due to the change of E_{LD} , the total energy consumption E_{Total} can be reduced.

T_P refers to the time interval for transmitting the laser at the HAR intervals. As shown in Figure 7, if the HAR is increased by narrowing T_P , the LiDAR sensor's power consumption increases as the accuracy of the object detection increases.

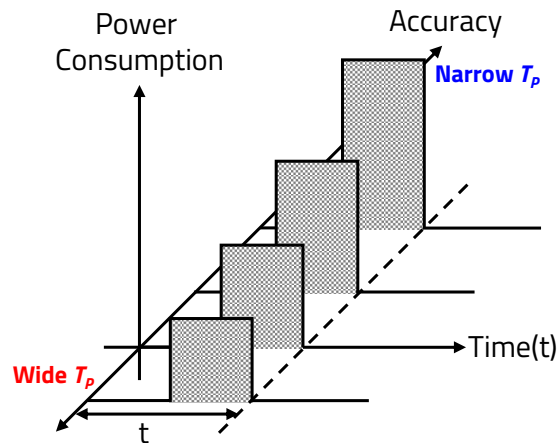


Figure 7. Relation of power consumption and accuracy.

In addition, if the HAR is decreased by widening T_p , the power consumption decreases as the accuracy decreases. Therefore, because T_p of the LD, which determines the HAR, and the accuracy of the object detection are proportional, power consumption increases as T_p narrows for the same period of time.

3.2. Proposed LiDAR Sensor

In this paper, we propose methods to efficiently reduce the sensor's power consumption by varying the HAR of the 16-channel scanning LiDAR sensor. The proposed LiDAR sensor is designed and manufactured for vehicles and has the specifications as shown in Table 1. As mentioned in Section 1, the proposed LiDAR sensor detects objects up to 150 m using a NIR 905 nm laser based on pulsed ToF technology. The proposed LiDAR communicates an external device using BroadR-Reach (BRR), which is an Ethernet for vehicle, and additionally has a controller area network (CAN) communication to enable connection with the vehicle's engine control unit (ECU). In addition, the proposed LiDAR sensor is designed to operate at 12 V, which is an operation voltage for vehicles, up to 36 V. Therefore, it can be driven at even more than 24 V, which is a power supply for a bus.

Table 1. Proposed LiDAR sensor specifications.

Model	Features	Specification
16 ch LiDAR	Channels	16 ch (Parallel layers)
	Technology	Pulsed ToF
	Source	NIR 905 nm
	HFoV	145°
	VFoV	9.6°
	Scanning frequency	30 Hz
	Angular resolution	H : 0.25° / V : 0.6°
	Range	≤150
	Interface	BroadR-Reach Ethernet / CAN / RS-232
	Viewer	Self-development using Qt
Operation voltage	10–36 VDC	
Power Consumption	≤7.5 W	

The LD of the proposed LiDAR sensor transmits a single-beam laser, which is the VFoV of 9.6°. The pulse width of the laser is 10 ns and frequency is about 86 kHz, when the HAR is 0.25°. A single 16-channel APD, which consist of 16 sensing cells, receives the laser reflected by the object into almost similar frequency as shown in Figure 8.

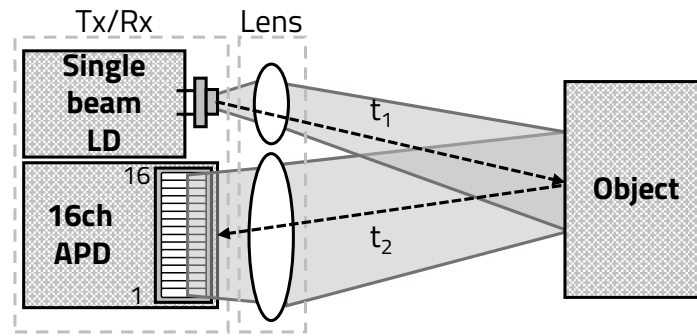


Figure 8. Structure of proposed LiDAR sensor's sensing.

Therefore, the proposed LiDAR sensor's VAR is determined by the APD's 16 sensing cells as 0.6° . The LiDAR sensor's HAR is determined by the number of the laser transmissions within the HFoV. When the motor is rotated at 30 Hz (=30 cycles), the LiDAR sensor takes about 33.33 ms to rotate at one cycle (360°), and a sensing angle of 145° takes about 13.43 ms. Therefore, N_x is determined as shown in Table 2 by the HAR as taking 13.43 ms.

Table 2. N_x depending on horizontal angular resolution (HAR).

HFoV ($^\circ$)	HAR ($^\circ$)	N_x	Term (μ s)
145	0.25	580	11.57
	0.3	483	13.89
	0.35	414	16.21
	0.4	362	18.54
	0.45	322	20.84
	0.5	290	23.14

As shown in Figure 9, the proposed LiDAR sensor that can measure more than 100 m uses the reflection mirror mounted on the BLDC motor, which rotates to 30 Hz and transmits a laser 580 times at 0.25° intervals—a basic HAR—within the HFoV of 145° .

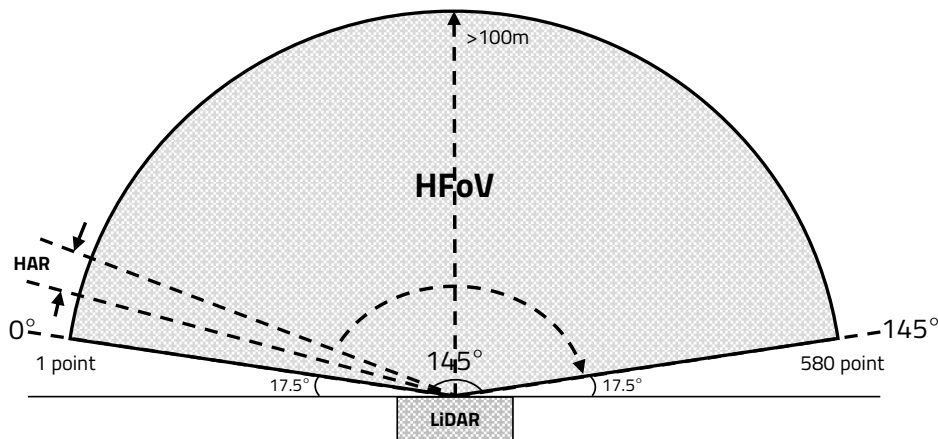


Figure 9. Horizontal field of view (HFoV) of LiDAR sensor.

As shown in Figure 10, the 16-channel LiDAR sensor, which detects the object, implements one frame using the VFoV of 9.6° and the HFoV of 145° .

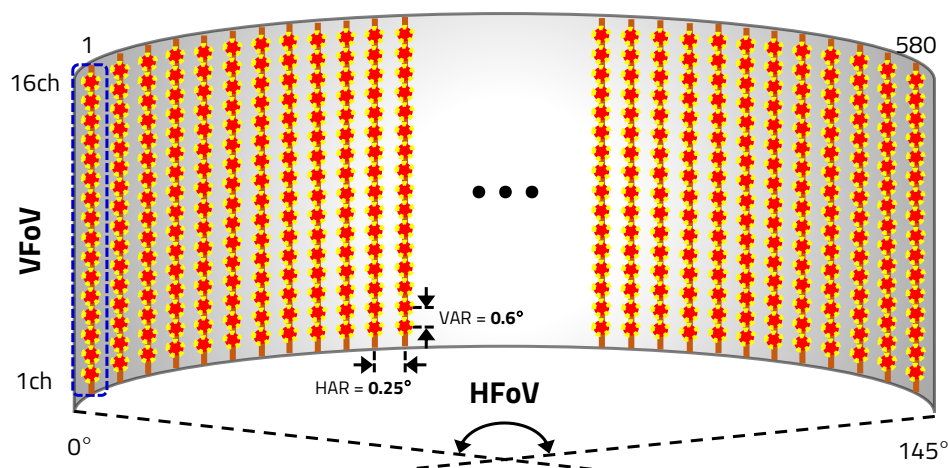


Figure 10. Point cloud of LiDAR sensor.

With these specifications, we propose methods to efficiently reduce the power consumption of the LiDAR sensor from two perspectives: the vehicle's speed and the sensor's surrounding environment. In terms of the vehicle's speed, the LiDAR sensor controls the HAR to reduce the dynamic power consumption. In terms of the sensor's surroundings, the LiDAR sensor goes into sleep mode to minimize the static power consumption.

3.2.1. Speed Detection-Based LiDAR Sensor Control

A LiDAR sensor with the same HAR, T_p , detects the object more accurately at a short distance than at a long distance because of the angle at which the laser is transmitted. Therefore, when considering the distance to the object, if the laser's HAR is low, the LiDAR sensor can be used for short-range object detection, and the higher the laser's HAR, the more suitable it will be for detecting long-range objects. We designed the LiDAR sensor so that the LD's T_p depends on the vehicle's speed, as depicted in Algorithm 1. When the vehicle's speed is faster than 100 km/h, the LiDAR sensor uses the maximum accuracy to detect distant objects at high speed. However, when the vehicle's speed is slower than 100 km/h, N_x is reduced for low-power operation. As shown in Table 3, when the vehicle's speed is faster than 100 km/h, the LiDAR sensor transmits the laser 580 times to the maximum number of laser transmissions ($N_{x.max}$) with 0.25° HAR. When the vehicle is driving at medium-high speed (80–100 km/h), the LiDAR sensor transmits the laser 483 times at 0.3° HAR, so our method reduces N_x by 16.73%. N_x is decreased by 28.62% with 414 laser transmissions and 0.35° HAR, when the vehicle's speed is medium (60–80 km/h). For medium-low speeds (40–60 km/h), the LD transmits the laser 362 times, which reduce N_x by 37.56%, and the HAR is 0.4° . If the vehicle's speed is slower than 40 km/h, then the minimum number of laser transmissions ($N_{x.min}$), 322, can decrease N_x by 44.48% with a 0.45° HAR.

Table 3. N_x depending on vehicle's speed.

Speed (km/h)	HAR ($^\circ$)	N_x	N_x Rate (%)
$S \geq 100$	0.25 (–)	580 (–)	100 (–)
$100 > S \geq 80$	0.3 (+0.05)	483 (–97)	83.23 (–16.73)
$80 > S \geq 60$	0.35 (+0.1)	414 (–166)	71.38 (–28.62)
$60 > S \geq 40$	0.4 (+0.15)	362 (–218)	62.41 (–37.56)
$40 > S \geq 0$	0.45 (+0.2)	322 (–258)	55.52 (–44.48)

Figure 11 shows the power consumption of the TDC and MP. The static power denoted as an area of the static current consumption, which is consumed continuously when the sensor is activated, is the same regardless of the power consumption control. However, the LD's N_x decreases according to

the vehicle's speed, and the dynamic power denoted as an area of the dynamic current consumption, which is the sum of the power required to transmit the data at the TDC and the power required to process the data at the MP, is decreased.

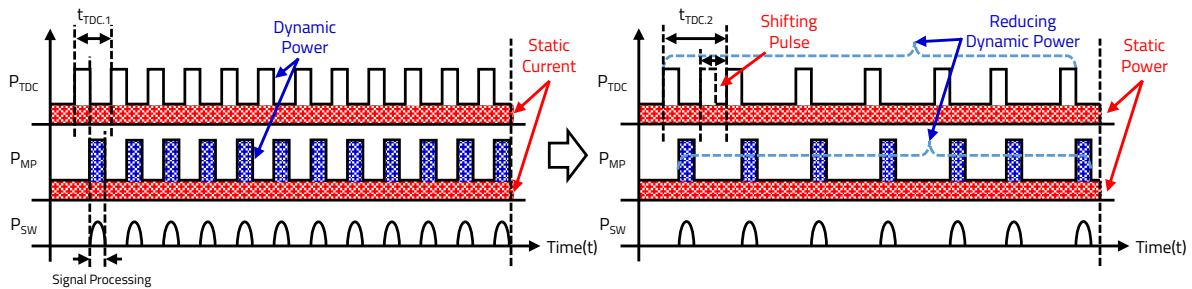


Figure 11. Power consumption of speed detection-based LiDAR sensor.

Algorithm 1: Speed detection-based accuracy control.

- 1 Goal: Determine N_x
 - 2 S : a vehicle's speed
 - 3 A : an accuracy of the sensor
 - 4 D : a sensing delay
 - 5 D_0 : a base sensing delay
 - 6 N_x : the number of the laser transmissions
 - 7 Function: SpeedBasedControl(S)
 - 8 $D = D_0$
 - 9 **if** $40 > S \geq 0$ **then**
 - 10 $A = 55.52\%$
 - 11 **else if** $60 > S \geq 40$ **then**
 - 12 $A = 62.41\%$
 - 13 **else if** $80 > S \geq 60$ **then**
 - 14 $A = 71.38\%$
 - 15 **else if** $100 > S \geq 80$ **then**
 - 16 $A = 83.23\%$
 - 17 **else**
 - 18 $A = 100\%$
 - 19 $N_x = 580 \times A$
-

3.2.2. Environment Sensing-Based LiDAR Sensor Control

The LiDAR sensor does not need to detect the surroundings with high HAR when the vehicle is stopped or when objects are not detected at very long distances. Based on the environmental detection results, the MP reduces the power consumption by entering sleep mode, which commands the LiDAR sensor to sleep. As shown in Figure 12, the LD of the LiDAR sensor transmits the laser at every cycle in the speed detection mode, and T_p varies depending on the vehicle's speed. However, because the LD transmits only one cycle out of five cycles in sleep mode, not only is T_p variable, but the static power consumption is also reduced. As shown in Figure 13, the time to detect only 145° out of the one cycle (360°) is 13.43 ms, and the time of the non-detection region, in which LD is not transmitted, is 153.24 ms. In addition, the LiDAR sensor in sleep mode transmits 290 times with 0.5° HAR, which is half at $N_{x,max}$ when the vehicle's speed is faster than 100 km/h, as shown in Table 4.

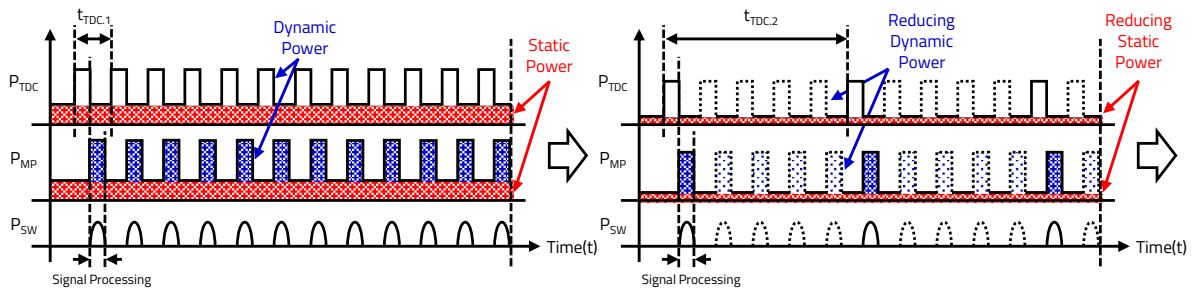


Figure 12. Power consumption of environment sensing-based LiDAR sensor.

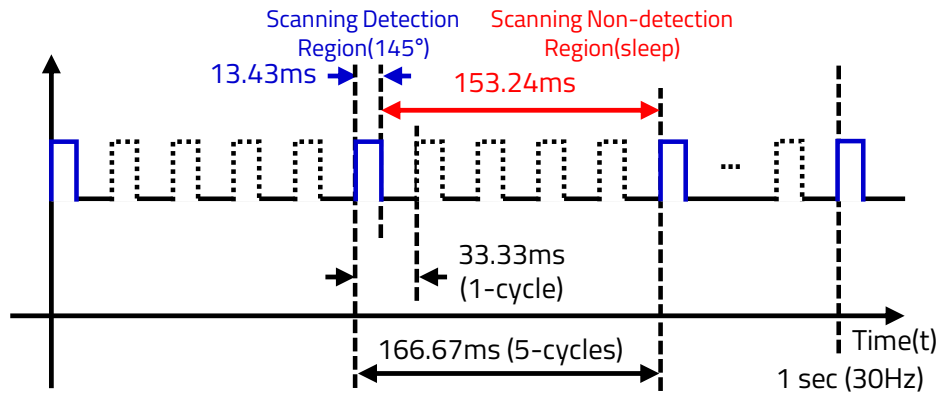


Figure 13. Time domain of sleep mode.

Table 4. N_x depending on vehicle’s surrounding environment.

Speed (km/h)	HAR (°)	N_x	N_x Rate (%)
$S \geq 100$	0.25 (-)	580 (-)	100 (-)
$100 > S \geq 80$	0.3 (+0.05)	483 (-97)	83.23 (-16.73)
$80 > S \geq 60$	0.35 (+0.1)	414 (-166)	71.38 (-28.62)
$60 > S \geq 40$	0.4 (+0.15)	362 (-218)	62.41 (-37.56)
$40 > S \geq 0$	0.45 (+0.2)	322 (-258)	55.52 (-44.48)
Sleep mode	0.50 (+0.25)	290 (-290)	50 (-50.00)

The environment sensing-based LiDAR sensor reduces the power consumption in two cases: when the vehicle is moving or not moving. When the vehicle is driving, the LiDAR sensor operates based on the method represented in Section 3.2.1, in which T_p is controlled by the vehicle’s speed. However, if the sensor does not detect any objects for a certain time period, the LiDAR sensor will determine that there are no objects around the vehicle, and it will enter sleep mode to minimize the detection speed and power consumption. The sensor will detect the surroundings when the vehicle stops or waits for a traffic signal. The LiDAR sensor enters sleep mode when the surrounding objects have not moved for a certain time period. In sleep mode, the LiDAR sensor regularly detects the surrounding environment every five cycles, and maintains the sleep mode if no object is detected. If the environment, which the sensor detects periodically, is changed or the vehicle starts to move, the LiDAR sensor returns to the active mode and detects objects with normal T_p , as depicted in Algorithm 2.

Algorithm 2: Environment sensing-based accuracy control.

```

1 Goal: Determine  $N_x$ 
2  $N_x$ : the number of the laser transmissions
3  $S$ : a vehicle's speed
4  $D$ : a sensing delay
5  $D_0$ : a base sensing delay
6  $d$ : a distance of the object
7  $k$ : a detection window
8  $\Delta$ : a margin of the detection
9  $A$ : an accuracy of the sensor

10 Function: EnvironmentBasedControl( $S, d_i$ )
11  $\{d_i\} = [d_{i-k}, d_{i-k+1}, \dots, d_i]$ 
12  $d_{av} = \frac{\text{sum}\{d_i\}}{k}$ 
13 if  $d_{av} + \Delta \geq d_i \geq d_{av} - \Delta$  then
14    $D = 5 \times D_0$ 
15   Sleep TDC, Processor at  $D$ 
16    $A = 20\%$ 
17 else
18   SpeedBasedControl( $S$ )
19  $N_x = 580 \times A$ 

```

4. Implementation and Experiment

For an experiment with the proposed algorithm, we designed private hardware based on a Zynq7020 processor (San Jose, CA, USA) and manufactured a LiDAR sensor module. To verify the LiDAR sensor, a test environment through the LiDAR sensor and viewer program was configured as shown in Figure 14a. The dedicated viewer program to check the operation status of the LiDAR sensor was implemented using the open source edition of the Qt framework and the point cloud library (PCL). In addition, the LiDAR sensor's power consumption was measured using a LiDAR sensor and a smart power debugger, a verification system, as shown in Figure 14b.

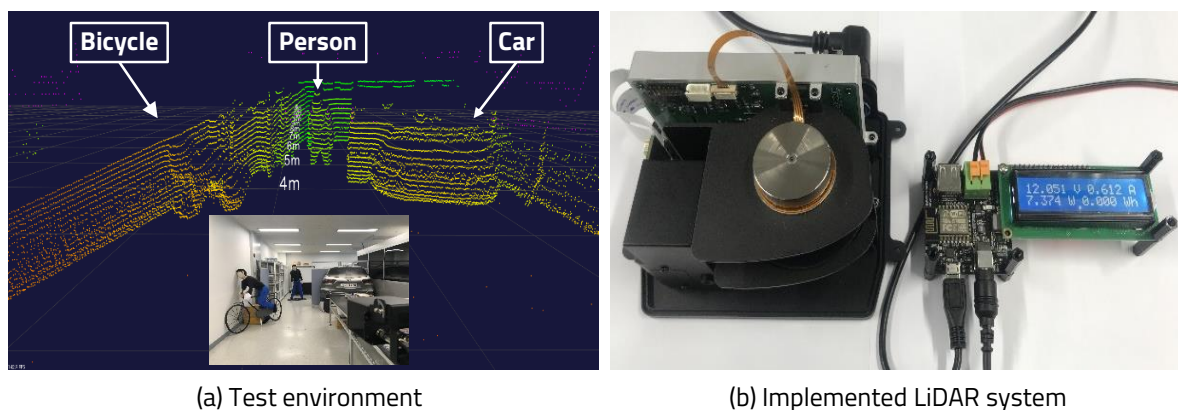


Figure 14. Test environment and implemented LiDAR system. (a) Test environment for LiDAR evaluation (bicycle, person, and car are detected). (b) Power consumption measurement setup for evaluating implemented LiDAR system.

The experiment was divided into two types, and the simulation results of the produced chip are shown based on the experimental results. First, the resulting change in T_P was compared after the experiment with variable T_P according to the variable HAR of the LiDAR sensor's operation. Second,

in order to confirm the effect of the proposed LiDAR sensor's algorithm, the variable HAR and the sleep mode are applied, and the LiDAR sensor's power consumption was measured to verify that the power consumption varied according to the HAR.

4.1. Power-Consumption Measurement of LiDAR Sensor

The following experiment results confirm the variation of T_P according to the variable HAR of the LiDAR sensor. Based on Table 2 as shown in Section 3.1.2, when the HAR of $N_{x,max}$ (580 times) is 0.25° , we confirmed that the LD transmits the laser every $11.57 \mu\text{s}$ through an oscilloscope. In the same way, data were extracted for T_P from 0.3° to 0.5° in sleep mode, as shown in Figure 15. The results confirmed that T_P increased as the HAR decreased.

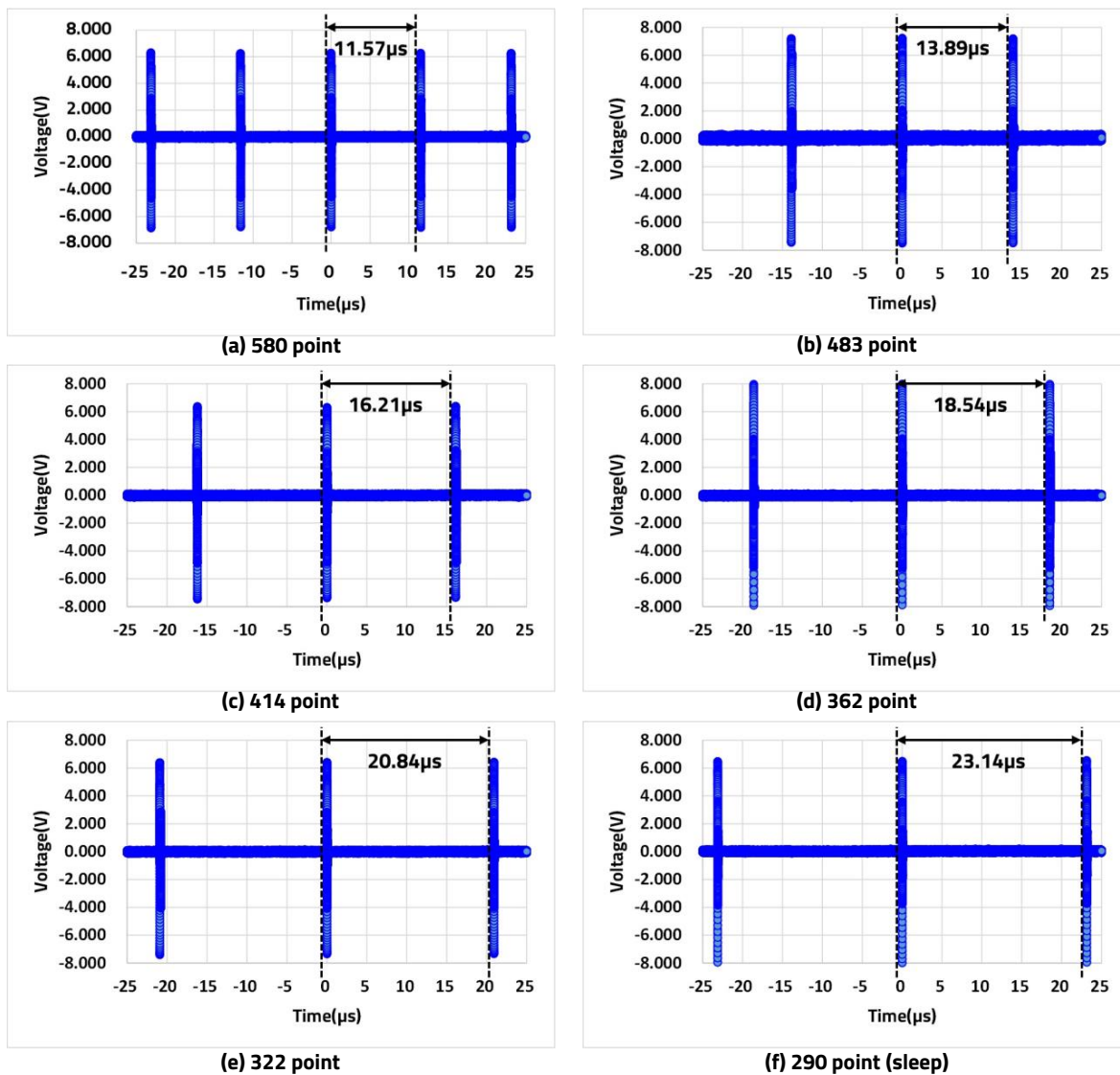


Figure 15. Comparison of T_P . (a) 580 laser transmissions at $11.57 \mu\text{s}$ intervals. (b) 483 laser transmissions at $13.89 \mu\text{s}$ intervals. (c) 414 laser transmissions at $16.21 \mu\text{s}$ intervals. (d) 362 laser transmissions at $18.54 \mu\text{s}$ intervals. (e) 322 laser transmissions at $20.84 \mu\text{s}$ intervals. (f) 290 laser transmissions at $23.14 \mu\text{s}$ intervals.

Additionally, the LiDAR sensor's HAR was varied by transmitting the laser every rotation, but in sleep mode, the laser was transmitted only once every five rotations to further reduce the power consumption in the environment sensing-based accuracy control mode. T_P was confirmed using an oscilloscope, as shown in Figure 16.

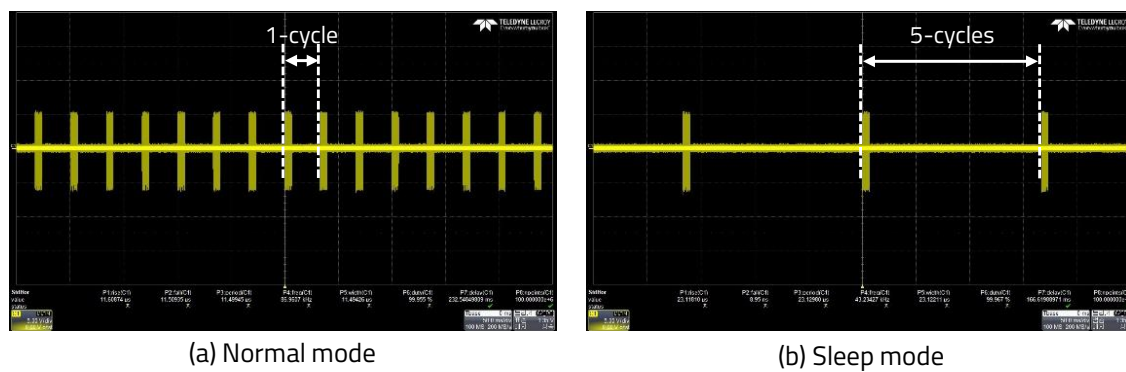


Figure 16. Comparison of T_P in normal and sleep mode. (a) Laser transmissions of N_x every cycle in normal mode. (b) Laser transmissions of 290 times for only 1-cycle in 5-cycles in sleep mode

Previously, the output of T_P was confirmed through experiments, and the LiDAR sensor's power consumption according to T_P was measured as shown in Figure 17. The measured results are divided into boot, motor (start, stabilization), and normality sections. The data for the actual boot and motor sections were considered invalid because it is the power use section before normality section. Only valid data of the normality section were extracted and expressed, as shown in Table 5.

Table 5. Power consumption depending on N_x .

N_x	Supply Voltage (V)	AC (A)	APC (W)	Reduction Rate (%)
No-load	12.054	0.578	6.971	-
580	12.055	0.617	7.442	100 (-)
483	12.055	0.615	7.409	99.56 (-0.44)
414	12.055	0.609	7.347	98.72 (-1.28)
362	12.056	0.606	7.308	98.21 (-1.79)
322	12.056	0.605	7.289	97.95 (-2.05)
Sleep mode	12.057	0.593	7.154	96.14 (-3.86)

In a red waveform of the normality section, an average current (AC) of 0.578 A and an average power consumption (APC) of 6.971 W were obtained using the LiDAR sensor's power consumption in the no-load state without driving the LD. The blue waveform shows the APC of each from 7.442 W to 7.154 W, from $N_{x,max}$ to $N_{x,min}$, with the LD mounted and in sleep mode.

As described above, the APC is reduced when varying N_x depending on the vehicle's speed. When the vehicle is driving at low speed, the power consumption is reduced because the HAR, controlled by N_x , is lowered by the algorithm of the speed detection-based LiDAR sensor control. In particular, the sleep mode is reduced by 3.86% of the power consumption as compared to $N_{x,max}$. The power consumption can be improved by varying the HAR according to the vehicle's speed. In addition, from the LD's point of view, while the APC of the LiDAR sensor in the no-load state is 6.971 W, the power difference for the LD excluding only the no-load APC from $N_{x,max}$ to $N_{x,min}$ is expressed as shown in Table 6. When N_x is 580 times, the difference in the average current (DAC) is 39.0 mA, and the difference in the average power consumption (DAPC) obtained by subtracting the APC at the no-load state, excluding from the APC at $N_{x,max}$, is 470.4 mW.

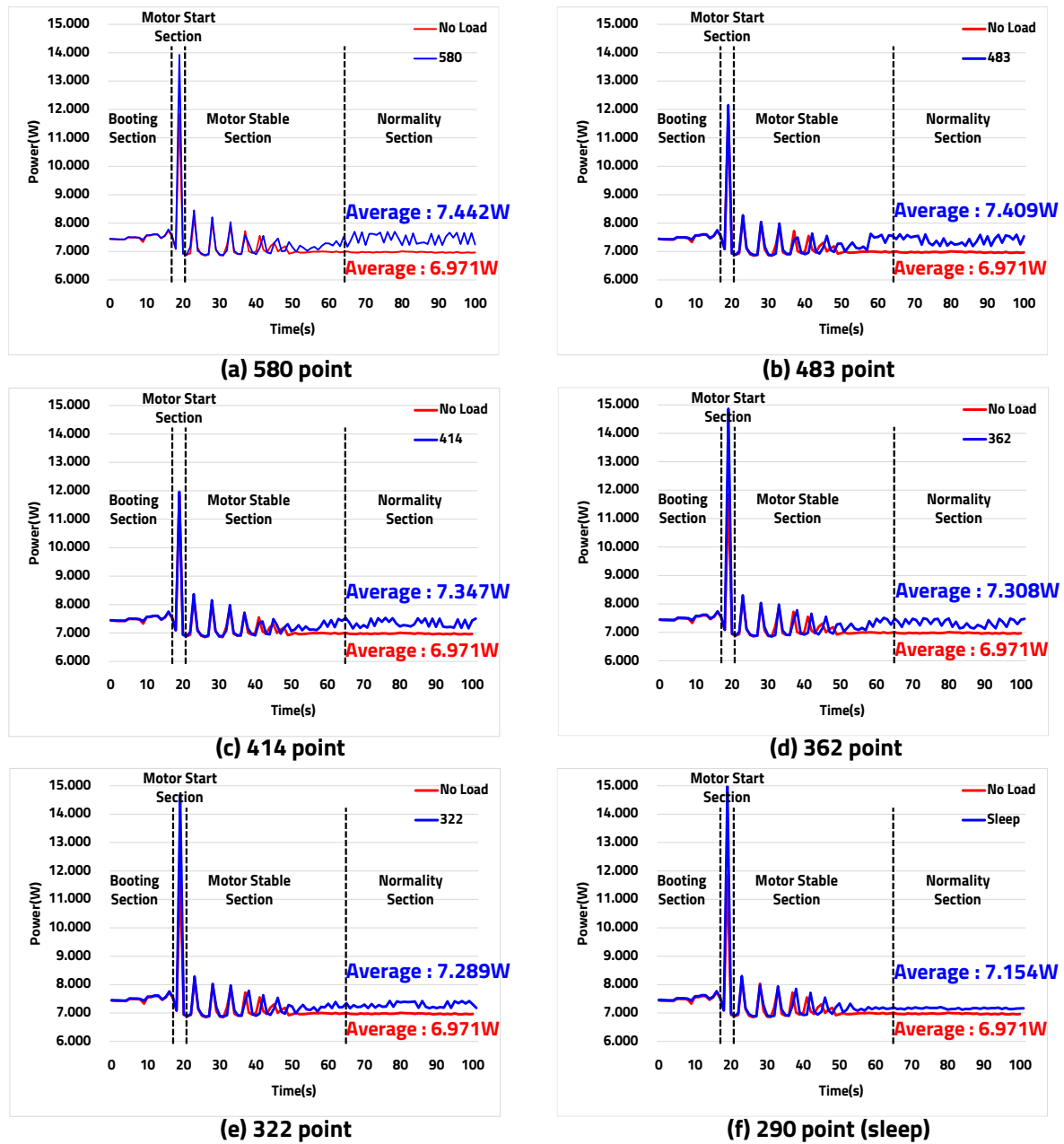


Figure 17. Comparison of power consumption depending on N_x . (a) Average power consumption graph of 7.442 W in 580 laser transmissions. (b) Average power consumption graph of 7.409 W in 483 laser transmissions. (c) Average power consumption graph of 7.347 W in 414 laser transmissions. (d) Average power consumption graph of 7.308 W in 362 laser transmissions. (e) Average power consumption graph of 7.289 W in 322 laser transmissions. (f) Average power consumption graph of 7.154 W in 290 laser transmissions.

Table 6. Power consumption rate of laser diode (LD).

N_x	DAC (mA)	DAPC (mW)	PRR (%)
580	39.0	470.4	100 (–)
483	36.3	437.8	93.08 (–6.92)
414	31.1	375.4	79.80 (–20.20)
362	27.9	337.1	71.67 (–28.33)
322	26.3	317.9	67.57 (–32.43)
Sleep mode	15.1	183.0	38.91 (–61.09)

In the sleep mode with $N_{x.min}$, the DAPC is 183.0 mW, which is 61.09% lower compared to $N_{x.max}$. In this case, the LD's power reduction rate (PRR) is changed step by step depending on the vehicle's speed. However, when N_x is 322 times, the PRR of sleep mode is approximately 1.8 times different from the PRR of 32.43%. As a result, the PRR in sleep mode is increased because it does not transmit the laser every cycle but only on one cycle out of five cycles. Therefore, the variable and HAR control of T_p being dependent on the vehicle's speed was verified by applying the speed detection algorithm, and the reduced power consumption of the LiDAR sensor was confirmed through the experimental results by additionally applying the environment-sensing algorithm.

The proposed LiDAR sensor's algorithm clearly has a risk factor of four cycles (153.24 ms) that does not detect an object in sleep mode during the environmental-sensing control. This issue is considered to be negligible because it immediately switches to active mode when surrounding conditions change in sleep mode when the vehicle is stop. In the future, further work on an adaptive mode that immediately exits sleep mode when an event occurs through dynamic control of sleep mode in conjunction with other sensors (images, RADAR sensors and etc.) of the autonomous vehicle is needed.

4.2. Chip Designed for the LiDAR Sensor

A designed chip was manufactured as shown in Figure 18 using the Global Foundries (Santa Clara, CA, USA) 55 nm process library, and it was implemented using approximately 540,000 gates, including an ARM core.

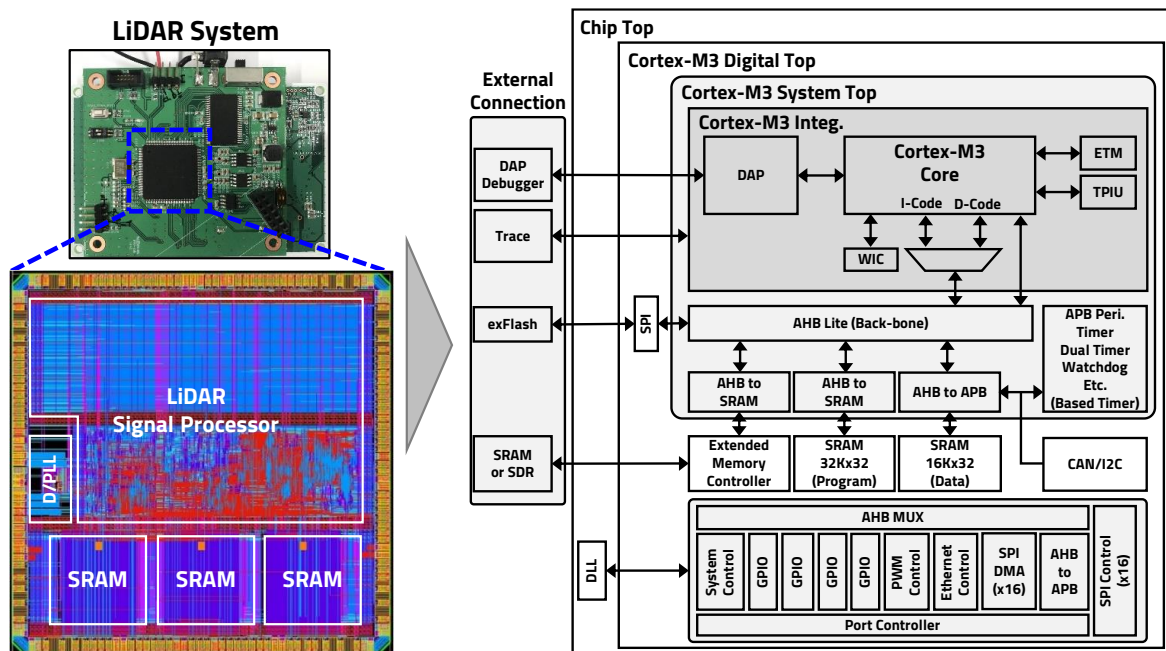


Figure 18. Designed microprocessor (MP) chip.

The chip is a MP with a built-in ARM Cortex-M3 (Cambridge, United Kingdom) that has 128 KB of program memory and 64 KB of data memory. In addition, we designed the chip to use external expansion memory in case the internal memory capacity is insufficient, which can be confirmed by the block diagram shown in Figure 18. A DLL designed on the chip can receive 4–24 MHz of clock from the outside and set the internal operation clock up to 160 MHz. The CPU fetches the program from the internal SRAM. The programming method was designed in two modes. The first mode directly programs the code to SRAM through I2C or debugger, and the second mode is executed by copying the program to SRAM by programming to external eFlash. An interface of the TDC is designed to support three types of TDC. The input can read data using 16 one-channel TDCs through SPI or read

data using one 16-channel TDC. In addition, data can be received via parallel transmission from the CMOS image sensor. The Ethernet port was designed with the SPI. An I2C slave controller was used to control a hardware register, and two modes were applied: a mode for accessing registers directly and one for access by communicating directly with the CPU. In addition, a timing control block for controlling the PWM was configured for the LD's T_p and to rotate the BLDC motor. Different timings could be controlled so that each block could operate independently. The PWM signal can generate desired waveforms by controlling the start latency, pulse width, pulse period, number of generated signals, and pulse hold. As described above, a dedicated chip was designed and manufactured for the LiDAR sensor, and the proposed algorithm will be applied to the manufactured chip for testing.

5. Conclusions

This paper proposes an algorithm to improve the inefficient constant operation method of conventional LiDAR sensors. Conventional LiDAR sensors inefficiently consume the operating power because they do not consider the vehicle's speed or the surrounding conditions. The proposed LiDAR sensor is implemented with software and hardware using the proposed algorithm to reduce the power consumption by varying the accuracy of a LiDAR sensor to be applied to electric and autonomous vehicles with limited power consumption. The proposed power-control algorithm operates according to two viewpoints: the vehicle's speed and the surrounding environment. First, the LiDAR sensor controls the laser's HAR based on the vehicle's speed to reduce the dynamic power consumption. Second, when the surrounding environment does not change for a certain time period, the proposed LiDAR sensor reduces the static power consumption by minimizing unnecessary detection through sleep mode. When the HAR was operated at 55.52% of $N_{x.max}$ at low speed using the proposed LiDAR sensor, the LD's APC was reduced by 32.43%, and when driving only one cycle per five cycles, the APC of the LD was reduced by 61.09%, and the HAR in sleep mode was reduced to 50% of $N_{x.max}$. The proposed LiDAR sensor applied the algorithm to control the HAR, which is T_p , according to the vehicle's speed, and successfully tested the LiDAR sensor using a verification system, which efficiently reduced the power consumption. Therefore, the proposed LiDAR sensor can flexibly cope with various vehicle environments and improve the efficiency of the operations with the applied algorithm. In addition, the manufactured chip for the LiDAR sensor uses the Global Foundries 55 nm CMOS process, and the designed processor area is 1,383,647 μm^2 and is about 540,000 gates. The chip has an ARM Cortex-M3 processor, and the designed processor will be tested using the proposed algorithm based on embedded software. The chip is expected to be completely redesigned with an on-chip MP and embedded software to optimize the power consumption as the environmental changes. In this paper, only the LD's power consumption of the LiDAR sensor was controlled by applying an algorithm that changes the HAR according to the vehicle's speed and detects the environment. Future research will be conducted to reduce the power consumption more efficiently by controlling parts other than the LD. It was determined that the proposed LiDAR sensor can be applied not only to the automotive industry but also to various fields, including the robot and drone industries, and that the power consumption algorithm can be applied in suitable ways for the field.

Author Contributions: S.L. designed the entire core architecture and performed the hardware/software implementation and experiments. D.L. performed the simulation and verification tasks. P.C. advised the low-power issues in terms of designing the analog sensor front-end circuits. D.P. had his role as corresponding author and the principle investigator for this research. All authors have read and agreed to the published version of the manuscript.

Funding: This work was supported by the Technology Innovation Program (10080079, The Development of low-cost LiDAR Sensor including Laser Diode and Semiconductor for Autonomous Car) funded By the Ministry of Trade, Industry & Energy(MOTIE, Korea). This research was supported by the Basic Science Research Program through the National Research Foundation of Korea(NRF) funded by the Ministry of Education(grant No. 2018R1D1A1B07041296). This research was supported by Basic Science Research Program through the National Research Foundation of Korea (NRF) funded by the Ministry of Science and ICT (NRF-2019R1A2C2005099), and Ministry of Education (NRF-2018R1A6A1A03025109), and BK21 Four project funded by the Ministry of Education, Korea (Started from Sept. 2020), and the EDA tool was supported by the IC Design Education Center(IDEC), Korea.

Conflicts of Interest: The authors declare no conflict of interest. The founding sponsors had no role in the design of the study; in the collection, analyses, or interpretation of data; in the writing of the manuscript, and in the decision to publish the results.

Abbreviations

The following abbreviations are used in this manuscript:

LiDAR	light detection and ranging
HAR	horizontal angular resolution
LD	laser diode
NIR	near-infrared ray
ToF	time-of-flight
APD	avalanche photo diode
TDC	time-to-digital converter
MP	microprocessor
AMCW	amplitude-modulated continuous-wave
FMCW	frequency-modulated continuous-wave
MEMS	microelectromechanical systems
OPA	optical phased array
RADAR	radio detection and ranging
VAR	vertical angular resolution
BLDC	brushless direct current
VFoV	vertical field of view
PWM	pulse width modulation
TMR	internal timer
HFoV	horizontal field of view
SPI	serial peripheral interface
OSC	oscillator
BRR	BroadR-Reach ethernet
CAN	controller area network
ECU	engine control unit
PCL	point cloud library
AC	average current
APC	average power consumption
DAC	difference in average current
DAPC	difference in average power consumption
PRR	power reduction rate

References

1. Basu, A.K.; Tatiya, S.; Bhattacharya, S. Overview of Electric Vehicles (EVs) and EV Sensors. In *Sensors for Automotive and Aerospace Applications*; Springer: Singapore, 2019; pp. 107–122.
2. Armstrong, K.; Das, S.; Cresko, J. The energy footprint of automotive electronic sensors. *Sustain. Mater. Technol.* **2020**, *25*, e00195.
3. Winner, H.; Hakuli, S.; Lotz, F.; Singer, C. *Handbook of Driver Assistance Systems*; Springer International Publishing: Amsterdam, The Netherlands, 2014; pp. 405–430.
4. Rasshofer, R.; Gresser, K. Automotive Radar and Lidar Systems for Next Generation Driver Assistance Functions. *Adv. Radio Sci. Kleinheubacher Berichte* **2005**, *3*, 205–209. [[CrossRef](#)]
5. Jo, K.; Kim, J.; Kim, D.; Jang, C.; Sunwoo, M. Development of Autonomous Car-Part I: Distributed System Architecture and Development Process. *IEEE Trans. Ind. Electron.* **2014**, *61*, 7131–7140. [[CrossRef](#)]
6. Hecht, J. Lidar for Self-Driving Cars. *Opt. Photonics News* **2018**, *29*, 26–35. [[CrossRef](#)]
7. Crouch, S. Advantages of 3D imaging coherent lidar for autonomous driving applications. In Proceedings of the 19th Coherent Laser Radar Conference, Okinawa, Japan, 18–21 June 2018.
8. Sarbolandi, H.; Plack, M.; Kolb, A. Pulse Based Time-of-Flight Range Sensing. *Sensors* **2018**, *18*, 1679. [[CrossRef](#)]

9. Theiß, S. Analysis of a Pulse-Based ToF Camera for Automotive Application. Master's Thesis, University of Siegen, Siegen, Germany, 27 March 2015.
10. Gokturk, S.; Yalcin, H.; Bamji, C. A Time-Of-Flight Depth Sensor-System Description, Issues and Solutions. In Proceedings of the 2004 IEEE Computer Society Conference on Computer Vision and Pattern Recognition, CVPR 2004, Washington, DC, USA, 27 June–2 July 2004; p. 35.
11. Amann, M.C.; Bosch, T.; Lescure, M.; Myllyla, R.; Rioux, M. Laser Ranging: A Critical Review of Unusual Techniques for Distance Measurement. *Opt. Eng.* **2001**, *40*, 10–19.
12. Behroozpour, B.; Sandborn, P.; Wu, M.; Boser, B. Lidar System Architectures and Circuits. *IEEE Commun. Mag.* **2017**, *55*, 135–142. [[CrossRef](#)]
13. Agishev, R.; Gross, B.; Moshary, F.; Gilerson, A.; Ahmed, S. Range-resolved pulsed and CWFM lidars: Potential capabilities comparison. *Appl. Phys. B* **2006**, *85*, 149–162. [[CrossRef](#)]
14. Feneyrou, P.; Leviandier, L.; Minet, J.; Pillet, G.; Martin, A.; Dolfi, D.; Schlotterbeck, J.P.; Rondeau, P.; Lacondemine, X.; Rieu, A.; et al. Frequency-modulated multifunction lidar for anemometry, range finding, and velocimetry—1. Theory and signal processing. *Appl. Opt.* **2017**, *56*, 9663–9675. [[CrossRef](#)]
15. Thakur, R. Scanning LIDAR in Advanced Driver Assistance Systems and Beyond. *IEEE Consum. Electron. Mag.* **2016**, *5*, 48–54. [[CrossRef](#)]
16. Mizuno, T.; Mita, M.; Kajikawa, Y.; Takeyama, N.; Ikeda, H.; Kawahara, K. Study of two-dimensional scanning LIDAR for planetary explorer. *Proc. SPIE* **2008**, *7106*. [[CrossRef](#)]
17. Yoo, H.; Druml, N.; Brunner, D.; Schwarzl, C.; Thurner, T.; Hennecke, M.; Schitter, G. MEMS-based lidar for autonomous driving. *e & i Elektrotechnik und Informationstechnik* **2018**, *135*, 408–415. [[CrossRef](#)]
18. Urey, H.; Holmstrom, S.; Baran, U. MEMS laser scanners: A review. *J. Microelectromech. Syst.* **2014**, *23*, 259–275.
19. Moss, R.; Yuan, P.; Bai, X.; Quesada, E.; Sudharsanan, R.; Stann, B.; Dammann, J.; Giza, M.; Lawler, W. Low-cost compact MEMS scanning LADAR system for robotic applications. *Proc. SPIE* **2012**, *8379*, 837903.
20. Gelbart, A.; Redman, B.; Light, R.; Schwartzlow, C.; Griffis, A. Flash lidar based on multiple-slit streak tube imaging lidar. *Proc. SPIE* **2002**, *4723*, 9–19.
21. Mcmanamon, P.; Banks, P.; Beck, J.; Huntington, A.; Watson, E. A comparison flash lidar detector options. *Proc. SPIE* **2016**, *9832*, 983202. [[CrossRef](#)]
22. Sun, J.; Timurdogan, E.; Yaacobi, A.; Hosseini, E.; Watts, M. Large-scale nanophotonic phased array. *Nature* **2013**, *493*, 195–199. [[CrossRef](#)]
23. Heck, M. Highly integrated optical phased arrays: Photonic integrated circuits for optical beam shaping and beam steering. *Nanophotonics* **2016**, *6*, 93–107. [[CrossRef](#)]
24. Park, D.; Youn, J.M.; Cho, J. A low-power microcontroller with accuracy-controlled event-driven signal processing unit for rare-event activity-sensing iot devices. *J. Sens.* **2015**, *2015*. [[CrossRef](#)]
25. Popa, C. Low-power low-voltage CMOS analog signal processing circuits using a functional core. In Proceedings of the 2016 IEEE International Conference on Electronics, Circuits and Systems (ICECS), Monte Carlo, Monaco, 11–14 December 2016; pp. 680–683.
26. Malik, M.; Homayoun, H. Big data on low power cores: Are low power embedded processors a good fit for the big data workloads? In Proceedings of the 2015 33rd IEEE International Conference on Computer Design (ICCD), New York, NY, USA, 18–21 October 2015; pp. 379–382.
27. Lorenzon, A.F.; Cera, M.C.; Beck, A.C.S. On the influence of static power consumption in multicore embedded systems. In Proceedings of the 2015 IEEE International Symposium on Circuits and Systems (ISCAS), Lisbon, Portugal, 24–27 May 2015; pp. 1374–1377.
28. Lee, Y.; Park, M. Power Consumption and Accuracy in Detecting Pedestrian Images on Neuromorphic Hardware Accelerated Embedded Systems. In Proceedings of the 2019 Tenth International Green and Sustainable Computing Conference (IGSC), Alexandria, VA, USA, 21–24 October 2019; pp. 1–4.
29. Anne, V.S.R.K.; Vadada, S.; Sharma, S.; Shareef, B.S.M.; Rao, C.H.S. Design challenges of a low power ARM based image processing sub system for a portable radar. In Proceedings of the 2017 2nd International Conference on Communication and Electronics Systems (ICCES), Coimbatore, India, 19–20 October 2017; IEEE: Piscataway, NJ, USA, 2017; pp. 193–198.

30. Song, C.; Yavari, E.; Singh, A.; Boric-Lubecke, O.; Lubecke, V. Detection sensitivity and power consumption vs. operation modes using system-on-chip based doppler radar occupancy sensor. In Proceedings of the 2012 IEEE Topical Conference on Biomedical Wireless Technologies, Networks, and Sensing Systems (BioWireleSS), Santa Clara, CA, USA, 15–18 January 2012; pp. 17–20.
31. Douillard, B.; Underwood, J.; Kuntz, N.; Vlaskine, V.; Quadros, A.; Morton, P.; Frenkel, A. On the segmentation of 3d LIDAR point clouds. In Proceedings of the 2011 IEEE International Conference on Robotics and Automation (ICRA), Shanghai, China, 9–13 May 2011; IEEE: Piscataway, NJ, USA, 2011; pp. 2798–2805.
32. Himmelsbach, M.; Mueller, A.; Lüttel, T.; Wünsche, H.J. LIDAR-based 3D object perception. In Proceedings of 1st International Workshop on Cognition for Technical Systems, Munich, Germany, 6–8 October 2008; Volume 1.
33. Liu, J.; Sun, Q.; Fan, Z.; Jia, Y. TOF lidar development in autonomous vehicle. In Proceedings of the 2018 IEEE 3rd Optoelectronics Global Conference (OGC), Shenzhen, China, 4–7 September 2018; pp. 185–190.
34. Comeron, A.; Munoz-Porcar, C.; Rocabenbosch, F.; Rodriguez-Gomez, A.; Sicard, M. Current Research in Lidar Technology Used for the Remote Sensing of Atmospheric Aerosols. *Sensors* **2017**, *17*, 1450. [[CrossRef](#)]
35. Sun, H. *A Practical Guide to Handling Laser Diode Beams*; Springer: Cham, Switzerland, 2015; Volume 147.
36. Arvani, F.; Carusone, T.C.; Rogers, E.S. Tdc sharing in spad-based direct time-of-flight 3d imaging applications. In Proceedings of the 2019 IEEE International Symposium on Circuits and Systems (ISCAS), Sapporo, Hokkaido, Japan, 26–29 May 2019; pp. 1–5.
37. Alahdab, S.; Mäntyniemi, A.; Kostamovaara, J. Review of a time-to-digital converter (TDC) based on cyclic time domain successive approximation interpolator method with sub-ps-level resolution. In Proceedings of the 2013 IEEE Nordic-Mediterranean Workshop on Time-to-Digital Converters (NoMe TDC), Perugia, Italy, 3 October 2013; pp. 1–5.
38. Song, J.; An, Q.; Liu, S. A high-resolution time-to-digital converter implemented in field-programmable-gate-arrays. *IEEE Trans. Nucl. Sci.* **2006**, *53*, 236–241. [[CrossRef](#)]



© 2020 by the authors. Licensee MDPI, Basel, Switzerland. This article is an open access article distributed under the terms and conditions of the Creative Commons Attribution (CC BY) license (<http://creativecommons.org/licenses/by/4.0/>).